Zhang, Y., et al., 2021, Magnetostratigraphy of U-Pb–dated boreholes in Svalbard, Norway, implies that magnetochron M0r (a proposed Barremian-Aptian boundary marker) begins at 121.2 ± 0.4 Ma: Geology, v. 49, https://doi.org/10.1130/G48591.1

SUPPLEMENTAL MATERIAL G48591.1 **Zhang et al.**

Magnetostratigraphy of U–Pb-dated boreholes in Svalbard, Norway, implies that magnetochron M0r (a proposed Barremian–Aptian boundary marker) begins at 121.2 ±0.4 Ma

Yang Zhang, James G. Ogg*, Daniel Minguez, Mark W. Hounslow, Snorre Olaussen, Felix M. Gradstein, and Selen Esmeray-Senlet

*E-mail: *jogg@purdue.edu*

This Supplemental Material contains:

1. Additional information on the lithostratigraphy and facies
2. Paleomagnetic and magnetostratigraphy methods and results, with Supplementary Figures S1-S4 (paleomagnetics)
3. Supplementary Tables S1-S5 (in a separate supplementary data file: Supplementary Tables S1-S5_Zhang-etal.xlsx)
4. Supplementary references cited

1. Additional information on the lithostratigraphy and facies

The DH boreholes in central Spitsbergen, Svalbard (Fig. 2D) are a series of fully cored wells, which were drilled to investigate the potential for CO_2 sequestration in the subsurface of Longyearbyen, Svalbard's largest settlement. The cores are currently stored at the University Centre in Svalbard (UNIS), and are included in the Svalbard Rock Vault initiative (*www.svalbox.no*) (Braathen et al., 2012). All the cores penetrate the Helvetiafjellet Formation and the lower part of the overlying Carolinefjellet Formation. The Helvetiafjellet Formation has a discontinuity onto the underlying Rurikfjellet Formation at a major erosion surface, known as the Barremian subaerial unconformity (e.g. Grundvåg et al., 2019; Fig. 2B).

The Lower Cretaceous basin fill in Svalbard accumulated as a response to long-term regional subsidence interrupted by crustal updoming with resulting uplift in the north caused by the opening of the Amerasian Basin and the onset of the High Arctic Large Igneous Province (HALIP) to the northeast (e.g., Gjelberg and Steel, 1995; Maher, 2001, Midtkandal and Nystuen, 2009; Grundvåg et al., 2019, 2020). The Festningen Member of the lowermost Helvetiafjellet Formation is dominated by coarse-grained quartzitic cross-bedded sandstones that are interpreted as braidplain deposits (Midtkandal and Nystuen, 2009; Grundvåg et al., 2019). The overlying Glitrefjellet Member consists of heterolithic deposits that accumulated in a wide range of paralic environments (Nemec, 1992; Grundvåg et al., 2019), broadly representing a low-angle fluvio-deltaic coastline. Detailed facies analysis in Engen (2018) concluded that the depositional environments of DH1 changed upward into an interdistributary bay facies in the uppermost part (Engen, 2018; and shown in Grundvåg et al., 2019, their fig. 11, based on data from the DH cores); thereby representing deposition under an overall increase in relative sea level and supporting the interpretations of trends described by other investigations (Nemec, 1992; Midtkandal and Nystuen, 2009; Grundvåg et al., 2017, 2020; Grundvåg and Olaussen 2017). The coastal plain during the deposition of the Helvetiafjellet Formation was subject to several relative sea level oscillations and/or shifting depocenters of sediment inputs (Midtkandal et al., 2007). The Helvetiafjellet Formation in the boreholes contains thin coal beds and soil horizons, in addition to scouring at the bases of some sandstone-filled channels (e.g., Grundvåg and Olaussen, 2017; Engen, 2018).

Sandstones in the Glitrefjellet Member show an upward increase in volcanoclastic fragments (Maher et al., 2004), including the 20-cm thick volcanic ash layer (i.e. a bentonite bed) reported in wells DH3, DH6 and DH7 (Corfu et al., 2013; Midtkandal et al., 2017; Grundvåg, written commun., 2020). Well correlation between DH3-DH7 (~50 m apart) and a lateral extrapolation westwards (over a distance of ca. 7 km) to DH1 place the bentonite just below a thick fluvial sandstone unit at about level 180 m in borehole DH1 (Fig. 2). The lateral extrapolation of the bentonite bed is based on the assumption that the Glitrefjellet Member coastal plain was characterized by relatively flat-lying chronostratigraphic timelines and a 'layer-cake'-type of stratigraphic architecture, as suggested by previous studies (e.g. Midtkandal and Nystuen, 2009; Grundvåg and Olaussen, 2017; Grundvåg et al., 2019). The bentonite is a direct evidence of volcanic activity attributed to the regionally extensive HALIP (Polteau et al., 2016).

The uppermost beds of the Helvetiafjellet Formation consist of wave-reworked mouth-bar sandstones capped by a conglomeratic lag deposit containing a mixture of lithic and siderite fragments (Engen, 2018; Grundvåg et al., 2019). The lower ca. 10 m of the Carolinefjellet Formation is an organic-rich shale as a regional flooding transformed the Helvetiafjellet Formation coastal plain into a shallow-shelf depositional setting (Grundvåg et al., 2019, 2020).

2. Paleomagnetic and magnetostratigraphy methods and results, with Supplementary Figures S1-S3 (paleomagnetics)

2.1. Rock magnetism

The intent of rock magnetic experiments in this study is to determine the carriers of natural remanence and to inform NRM demagnetization and characteristic remanence (ChRM) interpretations. A subset of specimens (n=11) spanning the DH1 core was chosen for isothermal remanent magnetization (IRM) acquisition and demagnetization experiments and coercivity modeling. Results from these procedures for representative specimens (#166.65 and #202.05) are shown in Figure S1.

IRM acquisition and coercivity modeling (Kruiver et al., 2001) indicate three populations of magnetic minerals: 1) A low-coercivity population, (Mean Coercivity, i.e., $B_{1/2}$ = 10–15 mT); 2) a mid-coercivity population ($B_{1/2}$ = 40–50 mT); and 3) a high coercivity population ($B_{1/2}$ = 250–350 mT). Thermal demagnetization of orthogonal IRMs (Lowrie, 1990) consistent with these ranges (x = 0–30 mT, y = 30–100 mT, and z = 100–1000 mT) characterizes the relative importance of each population as remanence carriers, as well as their thermal properties.

The low-coercivity component (0 mT < $B_{1/2}$ < 30 mT) demonstrates steep declines in magnetization following heating between room temperature and 250°C. Magnetization increases slightly at the ~275°C step, stabilizes between 275°C and 300°C, then declines steeply at 325°C, and monotonically thereafter until ~400°C. The mid-coercivity component (30mT < $B_{1/2}$ <100 mT) demonstrates relatively stable magnetizations between room temperature and 250ºC, and decreases steadily between 250ºC and 450°C. The high coercivity component (100 mT < $B_{1/2}$ < 1 T) is stable up to 300°C, declines steeply between 300 and ~350°C, and then stabilizes. All three components stabilize between roughly 400ºC and 550°C or decline monotonically over that range, before being nearly completely demagnetized at 580°C.

The coercivity and IRM results indicate mixed magnetic mineralogy in our samples. The high coercivity population accounts for a minor component of the SIRM (~10% according to the coercivity model); the component that survives a high unblocking temperature (>580ºC) is most probably from the hematite. Depending on grain size and crystal habit, pyrrhotite could have coercivities up to 1 T (Lowrie, 1990), although values between 10 and 125 mT are more commonly expected (Peters and Dekkers, 2003). Natural pyrrhotite specimens, similar to our specimens, also demonstrate declines in magnetization between room temperature and 325°C, with increases in magnetization at 280ºC to 300°C (Dekkers, 1989). Pyrrhotite can thus explain low and high coercivity thermal demagnetization behaviors. A second possibility is that the blocking temperature shoulders between 250ºC and 400ºC are caused by the oxidation of

maghemite (e.g., Channell and Xuan, 2009). Greigite, on the other hand, is not important in our samples, which would be a viable candidate over a tighter coercivity range (37–95 mT, 67 mT average, Peters and Dekkers, 2003). The rotational remanent magnetization (RRM) (Snowball, 1997) analysis demonstrates emphatically that no greigite exists in the studied samples from Helvetiafjellet Formation (Fig. S2). Magnetite explains the persistent magnetization up to 580ºC, and appears to dominate the mid-coercivity population ($B_{1/2}$ = 49 mT). Therefore, magnetite is the main phase of the primary magnetization carriers, with minor contributions in some samples from detrital pyrrhotite or maghemite.

Coercivity and Unblocking Temperature Analyses

Sample 166.65, IRM Acquisition & Demagnetization

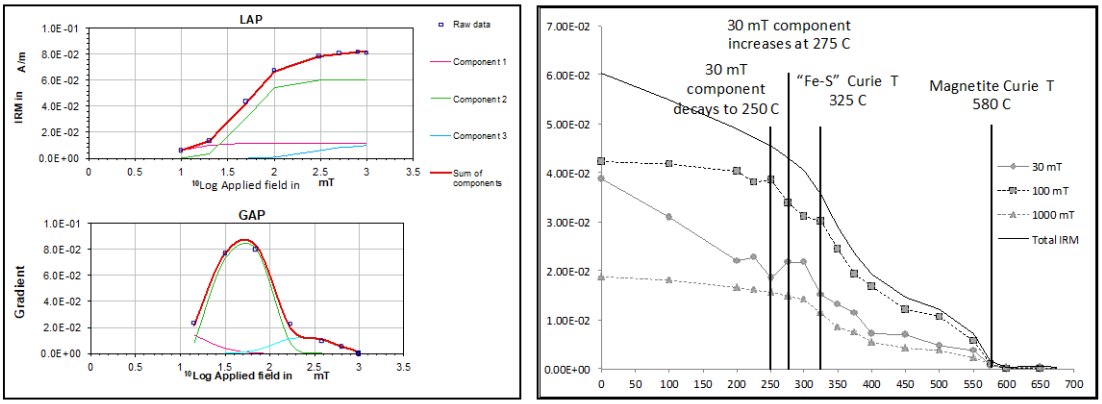

Sample 166.65, Coercivity Parameters

component	contribution	SIRM	log($B_{1/2}$)	$B_{1/2}$	DP
	%	A/m	mT	mT	mT
1	14.6	1.20E-02	1.00	10.0	0.30
2	73.2	6.00E-02	1.69	49.0	0.24
3	12.2	1.00E-02	2.40	251.2	0.30

Sample 202.05, IRM Acquisition & Demagnetization

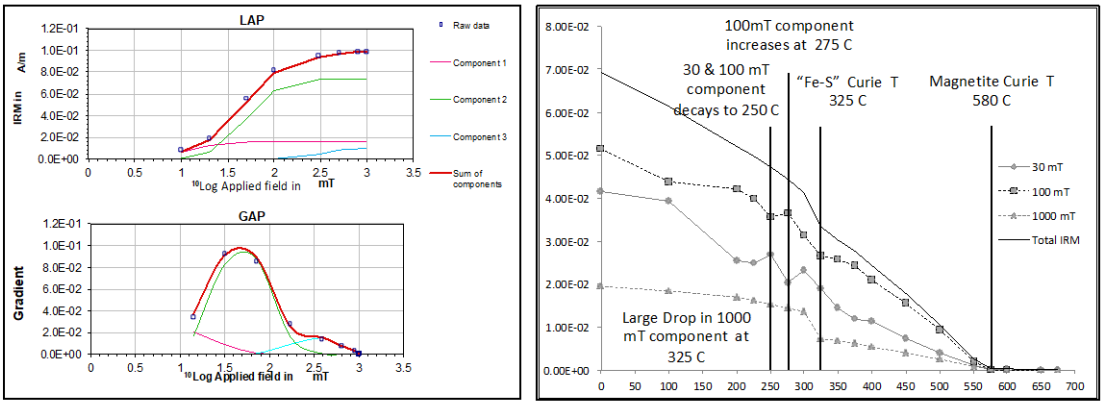

Sample 202.05, Coercivity Parameters

component	contribution	SIRM	log($B_{1/2}$)	$B_{1/2}$	DP
	%	A/m	mT	mT	mT
1	16.2	1.60E-02	1.10	12.6	0.30
2	73.7	7.30E-02	1.69	49.0	0.28
3	10.1	1.00E-02	2.50	316.2	0.25

Figure S1. Coercivity and unblocking temperature analyses of samples 166.65 and 202.05.

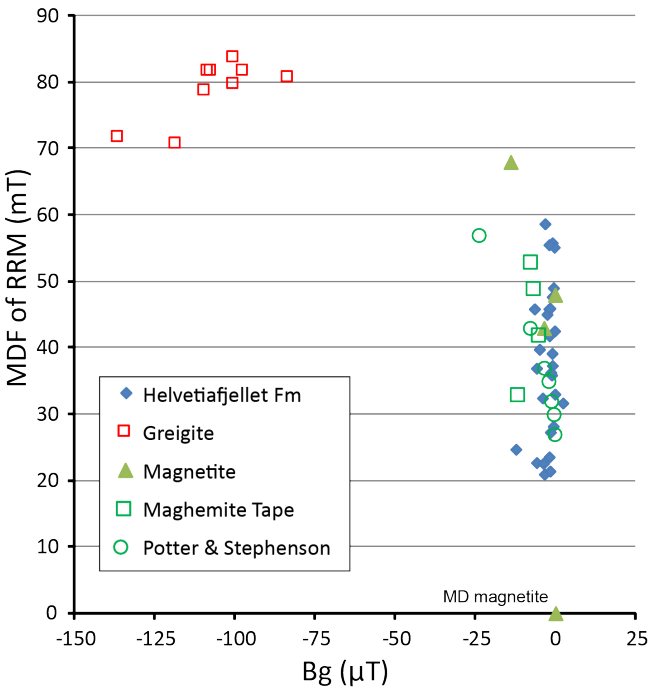

Figure S2. The rotational remanent magnetization (RRM) analysis. Greigite, magnetite and some maghemite data are from Snowball (1997); and Potter and Stephenson (1986) data used ball-milled natural magnetite. The data from Helvetiafjellet Formation in this study uses RRM at 5rps, and 100 mT, along with 100 uT bias for the ARM. The ARM used for the Bg is the rotational ARM. Measurements performed on a RAPID 2G.

2.2. Paleomagnetics

We sampled DH1 for magnetostratigraphy, rather than DH3, because the upper part of the Helvetiafjellet Formation and overlying Carolinefjellet Formation above the dated bentonite in DH3 had been distorted by permafrost, whereas the cored sediments in DH1 were intact. A total of 110 mini-cores were collected, of which 11 were selected as "pairs" to run comparative thermal/alternating AF field demagnetization before productive measurements. The thermal-only runs were performed using a Magnetic Measurements Ltd. (Aughton, Lancashire, UK) thermal demagnetizer, at increments ranging from 25–50°C until the magnetization was either too weak to measure or displayed unstable behavior (up to 450ºC). While the AF-only measurements were demagnetized using a Molspin tumbling alternating field demagnetizer (Molspin Ltd, Newcastle on Tyne, UK) at steps of 5 mT until 20 mT and then transitioned to 10 mT until 50–80 mT according to the demagnetization behaviors.

After examining the rock magnetic property and pilot sets data, a composite demagnetization scheme using thermal demagnetization to 200–300ºC (dictated by lithology) followed by AF was found to be most effective. Large changes in rock color (mineralogy) accompanied by surges in susceptibility and magnetic intensity were often seen above this critical range of thermal steps. The specimens were measured on a RAPID 2G magnetometer with noise level of ca. 1 x10^{-12} Am^2.

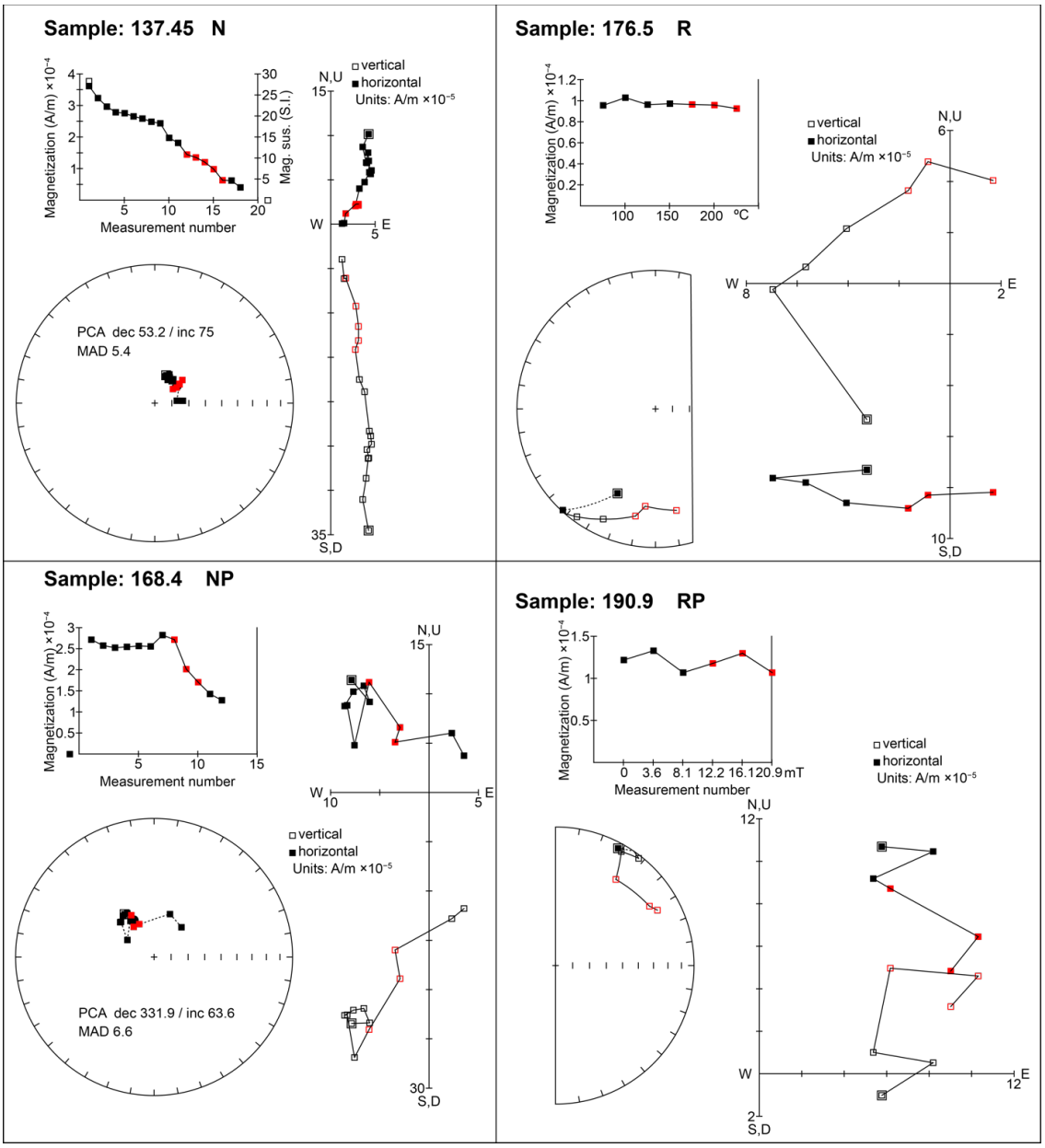

Figure S3. Examples of relatively good quality-rated (N/R for the upper two panels and NP/RP for the lower two panels) vector end-point diagrams of typical demagnetization behaviors. For lithologies and polarity interpretation of each sample, see Table S2 and S3.

Mean directions were determined using the PmagTool software (Hounslow, 2006). Quality ratings of 'N(R)', 'NP(RP)', 'NPP(RPP)', 'N?(R?)' or 'INT' were assigned to the ChRM directions and polarity interpretations according to a semi-subjective judgment of the behaviors of the magnetic vectors during the progressive demagnetization (Tables S2 and S3). We applied a 'P' tag ('RP' or 'NP') when the residual magnetization vector was considered close to attaining an endpoint before losing its residual magnetization or before experiencing a surge in susceptibility. The 'PP' tag was applied to samples that had a distinct trend toward the polarity

hemisphere to be considered indicative of the underlying polarity, but were judged to be too far from attaining an endpoint before dying to be used in statistics for computing a mean direction. The '?' qualifier was used to denote possible trends toward an underlying polarity, and 'INT' is either entirely uncertain or displayed an endpoint that was intermediate between the 'N' and 'R' poles. Examples of the quality ratings are illustrated in Fig. S3. Details on polarity interpretation are included in Supplementary Table S2. Examples of the good quality-rated demagnetization are shown in Fig. S3.

As well as the ChRM observed as the high stability component, in some specimens a down-directed component steeper than the ChRM was observed at low to mid stability ranges. This is interpreted as largely a Brunhes partial overprint, and was observed in 50 of the samples. The mean inclination (using marginal likelihood estimate; Enkin & Watson, 1996) of this Brunhes component is 76.8º (95% confidence interval 87.4º–71.6º) comparable to the expected Brunhes geocentric axial dipole (GAD) inclination of 84º (Fig. S4a). In 17 specimens an additional shallow inclination component was observed at the lowest stability (<200 ºC and < 15 mT) to demagnetization (Fig. S4c). This is inferred to be a storage remanence, since whilst aligned parallel with the core plug axis in some specimens, in others it is not, probably connected to the rotation of the core fragments during handling, storage and plugging.

For 21 of the specimens, we used the Brunhes overprint to re-orient the core (Brunhes declination rotated to 0º) enabling an overall mean direction to be determined (Fig. S4b), i.e., Dec.= 15.3°, Inc.= 65.5°, α_{95}= 11.3°, k= 8.9. This gives a pole (latitude 59ºN, longitude 175ºE) similar to other Cretaceous paleomagnetic data from Barents Sea region (Fig. S4d), giving support to the primary nature of our magnetization. The mean inclination of the ChRM is 57.8º (95% confidence interval 76.3º–51.8º). This compares with a steeper mean inclination of 71.4º (95% confidence interval 78.9º–69.1º) for Cretaceous volcanic paleomagnetic data from the Barents Sea region (Fig. S4). The shallower mean inclination may relate to the depositional nature of our magnetization (e.g., Kodama, 2012 and references therein). This pole was also used to determine the virtual geomagnetic pole (VGP) latitude in these specimens (Fig. 2 in the main text).

The remaining 29 specimens could not be satisfactorily re-oriented with the Brunhes component possibly due to component overlap with the storage component, which is evident by an elongation in the distribution of the Brunhes component along the plug-axis (Fig. S4a).

The obtained magnetostratigraphy (Fig. 2) allows a consistent match with the reference scale in GTS2012. Even though the fluvio-deltaic facies of the Helvetiafjellet Formation has a very irregular sediment accumulation punctuated by soil horizons and scour at bases of fluvial-distributary channels and though there is a low quality rating for many of the paleomagnetic samples, the combination of the subset of the higher-quality ChRMs and the other stratigraphic constraints do not allow another option to this main correlation to the magnetic polarity reference scale.

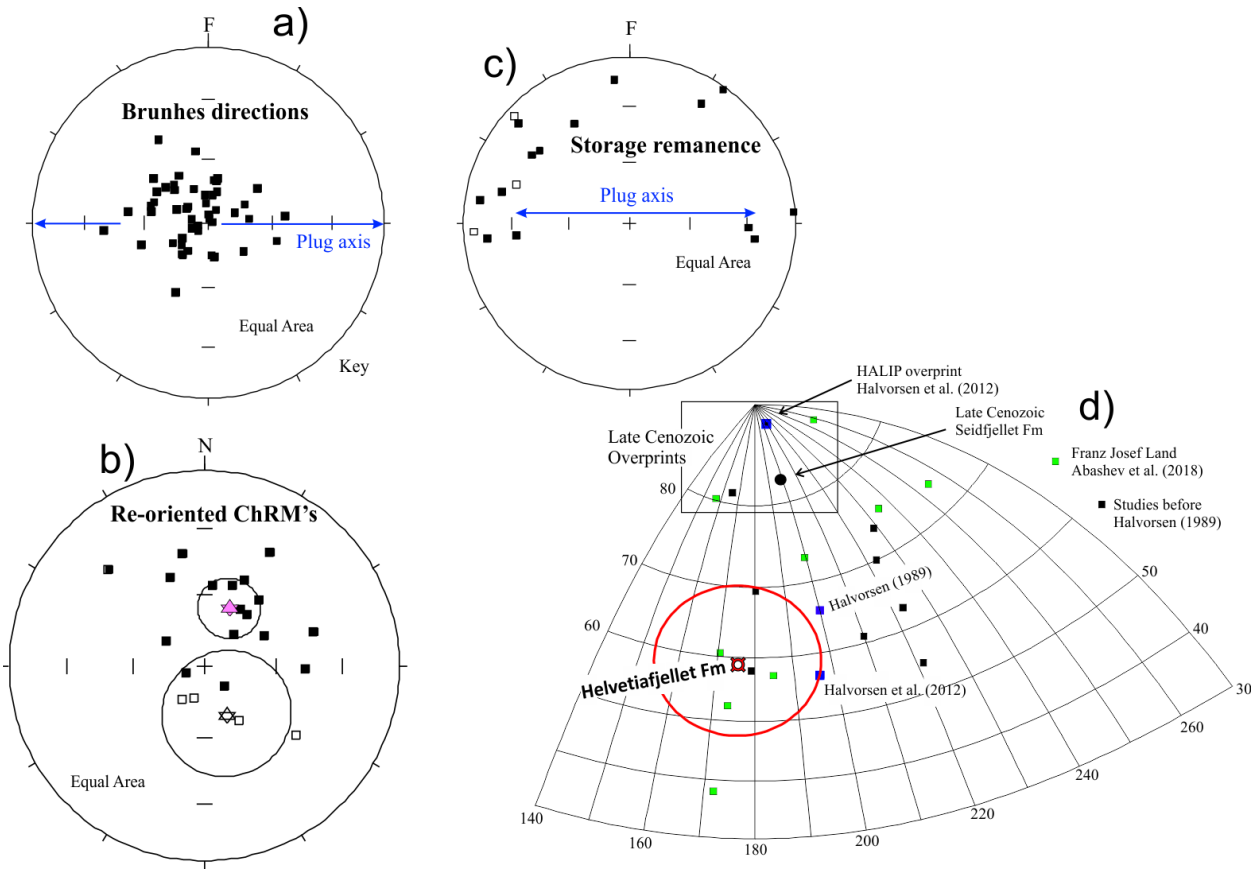

Fig. S4. Summary directional data obtained. a) The low to intermediate stability component interpreted as the Brunhes (declinations with respect to core-plug axis). b) The ChRM data that could be successfully re-oriented using the Brunhes component, with the mean (and 95% confidence cone) of the two polarities shown. c) The low stability component inferred to be a storage remanence, a sub-set of the directions plot along the core-plug axis, but not all. d) The mean pole (and 95% confidence cone) of the Helvetiafjellet Formation (in red) plotted with other Cretaceous paleomagnetic pole data from the Barents Sea region, and the late Cenozoic Seidfjellet Formation (black circle). All these data are from intrusives or lava units (lava data from Franz Josef Land; in green; Abashev et al. 2018). The Cretaceous data (ranging in age 160–110 Ma) largely relate to the High Arctic Large Igneous Province (HALIP; Senger et al., 2014), and like other Svalbard data has also been subject to late Cenozoic partial remagnetizations (Halvorsen, 1989; Halvorsen et al. 2012), which may in part be responsible for the large spread in poles. The overprint poles typically fall within the box shown when well defined (see also Hounslow and Nawrocki (2008) for discussion of Svalbard overprints). Our data falls close to the western end of this spread in good pole-data, which is close to the detailed re-assessments of HALIP data in Halvorsen et al. (2012) and Halvorsen (1989) (in blue). Some of the pre-1989 data and some of the data from Franz Josef Land may be partly contaminated with Cenozoic overprints, which are likely represented by the volcanic pole of the late Cenozoic Seidfjellet Formation on Svalbard. HALIP data not referenced in the figure are from the pole list in Hounslow and Nawrocki (2008).

3. Supplementary Tables S1-S5

(A separate supplementary data file: Supplementary Tables S1-S5_Zhang-etal.xlsx)

Table S1. References cited for sources of radiometric dates in Figure 1 of the main text

Table S2. Svalbard SH1 paleomagnetic sample descriptions, brief interpretations of each demagnetization result, characteristic directions (ChRM) and polarity rating

Table S3. Demagnetization steps of each sample

Table S4. Thermal demagnetization data of orthogonal IRMs

Table S5. Ages for three proposed markers for defining the Barremian-Aptian boundary

4. Supplementary references cited (excluding those in the main text)

Abashev, V.V., Metelkin, D. V., Mikhaltsov, N.E., Vernikovsky, V.A., and Bragin, V.Y., 2018, Paleomagnetism of traps of the Franz Josef Land Archipelago. Russian Geology and Geophysics, v. 59, no. 9, p. 1161-1181. https://doi.org/10.1016/j.rgg.2018.08.010

Braathen, A., et al. (23 authors), 2012, The Longyearbyen CO_2 Lab of Svalbard, Norway - initial assessment of the geological conditions for CO_2 sequestration: Norwegian Journal of Geology, v. 92, p. 353–376. https://njg.geologi.no/images/NJG_articles/NJG_4_2012_1Braathen_PR.pdf

Channell, J.E.T, and Xuan, C., 2009, Self-reversal and apparent magnetic excursions in Arctic sediments: Earth and Planetary Science Letters, v. 284, no. 1-2, p. 124-131. https://doi.org/10.1016/j.epsl.2009.04.020

Dekkers, M.J., 1989, Magnetic properties of natural pyrrhotite. II. High-and low-temperature behaviour of Jrs and TRM as function of grain size: Physics of the Earth and Planetary Interiors, v. 57, no. 3-4, p. 266-283. https://doi.org/10.1016/0031-9201(89)90116-7

Engen, T.M., 2018, A sedimentological study of the Lower Cretaceous Glitrefjellet Member, Svalbard [M.S. Thesis]: UiT The Arctic University of Norway), 139 p. https://munin.uit.no/handle/10037/12826.

Enkin, R.J., and Watson, G.S., 1996, Statistical analysis of palaeomagnetic inclination data. Geophysical Journal International, v. 126, no. 2, p. 495-504. https://doi.org/10.1111/j.1365-246X.1996.tb05305.x

Gjelberg, J., and Steel, R.J., 1995, Helvetiafjellet formation (Barremian-Aptian), Spitsbergen: characteristics of a transgressive succession: Norwegian Petroleum Society Special Publications, v. 5, p. 571–593. https://doi.org/10.1016/S0928-8937(06)80087-1

Grundvåg, S.A., and Olaussen, S., 2017, Sedimentology of the Lower Cretaceous at Kikutodden and Keilhaufjellet, southern Spitsbergen: implications for an onshore–offshore link: Polar Research, v. 36, p. 1302124. https://doi.org/10.1080/17518369.2017.1302124.

Grundvåg, S.-A., Marin, D., Kairanov, B., Śliwińska, K.K., Nøhr-Hansen, H., Jelby, M.E., Escalona, A., and Olaussen, S., 2017, The Lower Cretaceous succession of the northwestern Barents Shelf: Onshore and offshore correlations: Marine and Petroleum Geology, v. 86, p. 834–857. https://doi.org/10.1016/j.marpetgeo.2017.06.036

Grundvåg, S.-A., Jelby, M.E., Olaussen, S., and Śliwińska, K.K., 2020, The role of shelf morphology on storm-bed variability and stratigraphic architecture, Lower Cretaceous, Svalbard: Sedimentology, article #12791, 42 pp., https://doi.org/ 10.1111/sed.12791.

Halvorsen, E., 1989, A paleomagnetic pole position of Late Jurassic/Early Cretaceous dolerites from Hinlopenstretet, Svalbard, and its tectonic implications: Earth and Planetary Science Letters, v. 94, no. 3-4, p. 398-408. https://doi.org/10.1016/0012-821X(89)90156-8

Halvorsen, E., Løvlie, R., Andresen, A., Polteau, S., Walderhaug, H., and Faleide, J., 2012, Complete Cenozoic remagnetization of Cretaceous sills and lavas from the High Arctic Large Igneous Province (HALIP) on Svalbard imposed during faulting and burial/uplift. EGU General Assembly, Vienna Conference Abstracts, v. 14, p. 8302.

Hounslow, M.W., and Nawrocki, J., 2008, Palaeomagnetism and magnetostratigraphy of the Permian and Triassic of Spitsbergen: a review of progress and challenges: Polar Research, v. 27, no. 3, p. 502-522. https://doi.org/10.1111/j.1751-8369.2008.00075.x

Hounslow, M.W., 2006. PMagTools version 4.2- a tool for analysis of 2-D and 3-D directional data. https://doi.org/10.13140/RG.2.2.19872.58880.

Kodama, K.P., 2012, Paleomagnetism of Sedimentary Rocks: Process and Interpretation, Wiley-Blackwell. 184 p.

Kruiver, P.P., and Passier, H.F., 2001, Coercivity analysis of magnetic phases in sapropel S1 related to variations in redox conditions, including an investigation of the S ratio: Geochemistry, Geophysics, Geosystems, v. 2, no. 12, article #2001GC000181, p. 1-21. https://doi.org/10.1029/2001GC000181

Lowrie, W., 1990, Identification of ferromagnetic minerals in a rock by coercivity and unblocking temperature properties: Geophysical Research Letters, v. 17, no. 2, p. 159-162. https://doi.org/10.1029/GL017i002p00159

Maher Jr., H.D., 2001, Manifestations of the Cretaceous High Arctic Large Igneous Province in Svalbard: The Journal of Geology, v. 109, p. 91–104. https://doi.org/10.1086/317960.

Maher, H.D., Hays, T., Shuster, R., and Mutrux, J. 2004, Petrography of the Lower Cretaceous sandstones of Spitsbergen: Polar Research, v. 23, p. 147–165. https://doi.org/10.1111/j.1751-8369.2004.tb00005.x

Menegatti, A.P., Weissert, H., Brown, R.S., Tyson, R.V., Farrimond, P., Strasser, A., and Caron, M., 1998, High-resolution $\delta^{13}C$ stratigraphy through the early Aptian "Livello Selli" of the Alpine Tethys: Paleoceanography, v. 13, no. 5, p. 530-545. https://doi.org/10.1029/98PA01793

Midtkandal, I., and Nystuen, J.P., 2009, Depositional architecture of a low-gradient ramp shelf in an epicontinental sea: the lower Cretaceous of Svalbard: Basin Research, v. 21, p. 655–675. https://doi.org/10.1111/j.1365-2117.2009.00399.x.

Midtkandal, I., Nystuen, J.P., and Nagy, J., 2007, Paralic sedimentation on an epicontinental ramp shelf during a full cycle of relative sea-level fluctuation; the Helvetiafjellet Formation in Nordenskiöld land, Spitsbergen: Norsk Geologisk Tidsskrift, v. 87, p. 343-359. https://foreninger.uio.no/ngf/ngt/pdfs/NJG_87_343-359.pdf

Nemec, W. 1992: Depositional controls on plant growth and peat accumulation in a braidplain delta environment: Helvetiafjellet Formation (Barremian-Aptian), Svalbard. In: McCabe, P.J., and Parish, J.T., eds., Controls on the Distribution and Quality of Cretaceous Coals. Geological Society of America Special Paper, v. 267, p. 209–226. https://doi.org/10.1130/SPE267-p209

Peters, C., and Dekkers, M., 2003, Selected room temperature magnetic parameters as a function of mineralogy, concentration and grain size: Physics and Chemistry of the Earth, Parts A/B/C, v. 28, no. 16-19, p. 659-667. https://doi.org/10.1016/S1474-7065(03)00120-7

Potter, D., and Stephenson, A., 1986, The detection of fine particles of magnetite using anhysteretic and rotational remanent magnetizations: Geophysical Journal International, v. 87, no. 2, p. 569-582. https://doi.org/10.1111/j.1365-246X.1986.tb06638.x

Senger, K., Tveranger, J., Ogata, K., Braathen, A., and Planke, S., 2014, Late Mesozoic magmatism in Svalbard: A review: Earth-Science Reviews, v. 139, p. 123-144. https://doi.org/10.1016/j.earscirev.2014.09.002

Snowball, I.F., 1997, The detection of single-domain greigite (Fe3S4) using rotational remanent magnetization (RRM) and the effective gyro field (Bg): mineral magnetic and palaeomagnetic applications: Geophysical Journal International, v. 130, no. 3, p. 704-716. https://doi.org/10.1111/j.1365-246X.1997.tb01865.x